NASA Technical Memorandum 86985

Unified Constitutive Material Models for Nonlinear Finite-Element Structural Analysis

A. Kaufman
Lewis Research Center
Cleveland, Ohio

J.H. Laflen
General Electric Company
Cincinnati, Ohio

and

U.S. Lindholm
Southwest Research Institute
San Antonio, Texas

Prepared for the
Twenty-first Joint Propulsion Conference
cosponsored by the AIAA, SAE, and ASME
Monterey, California, July 8–10, 1985

NASA

UNIFIED CONSTITUTIVE MATERIAL MODELS FOR NONLINEAR FINITE-ELEMENT STRUCTURAL ANALYSIS

by

A. Kaufman
National Aeronautics and Space Administration
Lewis Research Center
Cleveland, Ohio

J.H. Laflen
General Electric Company
Cincinnati, Ohio

and

U.S. Lindholm
Southwest Research Institute
San Antonio, Texas

Abstract

Unified constitutive material models were developed for structural analyses of aircraft gas turbine engine components with particular application to isotropic materials used for high-pressure stage turbine blades and vanes. Forms or combinations of models independently proposed by Bodner and Walker were considered in this study. These theories combine time-dependent and time-independent aspects of inelasticity into a continuous spectrum of behavior. This is in sharp contrast to previous classical approaches that partition inelastic strain into uncoupled plastic and creep components. Predicted stress-strain responses from these models were evaluated against monotonic and cyclic test results for uniaxial specimens of two cast nickel-base alloys, B1900+Hf and René 80. Tension-torsion test results for René 80 and Hastelloy X alloys were used to evaluate multiaxial stress-strain cycle predictions. The unified models, as well as appropriate algorithms for integrating the constitutive equations, were implemented in finite-element computer codes.

Introduction

This paper discusses the development of unified constitutive material models and of compatible finite-element computer codes for the structural analysis of gas turbine engine hot section components. This effort constitutes a different approach for nonlinear structural analysis which has heretofore been based on classical plasticity theory with uncoupled creep equations. Previous analytical studies of hot section components such as turbine blades[1] and combustor liners[2] have demonstrated that existing nonlinear finite-element computer codes based on classical methods do not accurately predict the cyclic response of the structure.

The unified constitutive theories considered in this study encompass time-dependent and time-independent aspects of inelasticity including plasticity, creep and stress relaxation. These theories avoid the noninteractive summation of inelastic strain into plastic and creep components or specifying yield surfaces to partition stress space into elastic and elastic-plastic regions. In eliminating these overly simplified assumptions of classical theory, unified models can more realistically represent the behavior of materials under cyclic loading conditions and high temperature environments.

Results are reported for the first 18 months of a 4 yr NASA-sponsored program to develop inelastic structural analysis methods based on unified constitutive theories. This work is being performed under two NASA contracts; one with the General Electric Company and the other a joint effort of Southwest Research Institute and Pratt & Whitney. Model development is directed toward the prediction of the structural response of initially isotropic, cast nickel-base alloys for the temperatures and strain ranges characteristic of air-cooled turbine blades and vanes in advanced gas turbine engines.

After extensive review and evaluation of unified theories which have been suggested in the literature, those proposed by Bodner[3] and Walker[4] were selected for further study and development. Both of these theories were significantly revised by their authors during the course of and as a result of this program. Forms or combinations of these two models, as well as numerical methods for integrating the constitutive equations, have been implemented in two finite-element computer codes; by G.E. in a modular form in a new code specifically developed for a unified theory and by P&W in a stand-alone module for use with general purpose codes such as MARC.

Both programs followed essentially the same experimental work plan. This consisted of uniaxial and multiaxial tests to establish data bases, develop efficient procedures for determining the material constants and evaluate the candidate models. The alloys tested were René 80 in the G.E. program and B1900+Hf in the SwRI/P&W program. More than 30 uniaxial, isothermal, strain-controlled tests were performed under various strain rates, temperatures, alternating-to-mean strain ratios and hold times. The tests were continued until cyclic saturation was achieved. In addition, three uniaxial thermomechanical cyclic tests were conducted to study the models under nonisothermal conditions. Most of the multiaxial tests involved tension-torsion testing although G.E. also performed some cyclic tests on notched bar specimens to simulate tension-tension stress fields. Comparisons of model multiaxial predictions are shown for René 80 and for previously conducted tension-torsion test results for

Hastelloy X alloy. As a final demonstration of the unified analytical methods, cyclic structural analyses will be performed for an aircooled turbine blade or vane airfoil under simulated engine operating conditions.

Constitutive Models

The initial effort in this program was to survey and evaluate unified constitutive theories proposed in the literature. Only those theories were considered that incorporated time-independent (plasticity) and time-dependent (creep) aspects of inelastic behavior in a single inelastic strain rate term. Also excluded from consideration were theories which required a yield surface.

The criteria used in screening candidate constitutive theories were (1) ability to accurately represent the cyclic inelastic behavior of an isotropic, high-temperature superalloy, (2) applicability over the temperature and strain ranges of interest for aircooled turbine blades and vanes and typical mission cycles of advanced airbreathing engines, (3) capability of extension to multiaxial stress states and anisotropic materials, (4) reasonableness of material property testing requirements and ease of determining model constants, and (5) integrability of constitutive equations for implementation in finite-element computer codes.

Most unified models can be described by a set of constitutive equations that have the basic form

$$\frac{(\underset{\sim}{S} - \underset{\sim}{\alpha})}{K} = f(\dot{\underset{\sim}{\varepsilon}}_I) \tag{1}$$

$$\dot{K} = h_1(K)\dot{\underset{\sim}{\varepsilon}}_I - r_1 \tag{2}$$

$$\dot{\underset{\sim}{\alpha}} = h_2(\underset{\sim}{\alpha})\dot{\underset{\sim}{\varepsilon}}_I - d(\underset{\sim}{\alpha})|\dot{\underset{\sim}{\varepsilon}}_I| - r_2 \tag{3}$$

Equation (1) is a flow law relating the inelastic strain rate and the stresses where $\underset{\sim}{S}$ and $\underset{\sim}{\varepsilon}_I$ are deviatoric stress and inelastic strain rate tensors. The tensor internal variable, $\underset{\sim}{\alpha}$, defines the kinematic or directional hardening (the Bauschinger effect) and is frequently referred to as a back stress. K is a scalar internal variable, commonly called a drag stress, which defines the isotropic hardening. Temperature effects on the inelastic strain rate are generally taken into account by considering some of the material constants of the constitutive model to be temperature dependent. Equations (2) and (3) are evolutionary equations describing the growth laws for the internal variables. Most evolutionary equations for the back stress-drag stress type of model include both hardening and recovery terms where h_1 and h_2 are functions describing the hardening, d is a dynamic recovery function and r_1 and r_2 are static thermal recovery functions. Almost all back stress-drag stress models use the inelastic strain rate, $\dot{\varepsilon}_I$, as the hardening criterion. About a dozen unified theories which have been proposed in the literature were considered in the survey. There were substantial differences among the models in the functional relationships used in the constitutive equations.

The major exception to the basic form of Eqs. (1) to (3) is the Bodner model. The flow law for this model is of the form

$$\dot{\underset{\sim}{\varepsilon}}_I = D \exp\left[-\frac{1}{2}\left(\frac{Z^2}{3J_2}\right)^n\right]\frac{\underset{\sim}{S}}{\sqrt{J_2}} \tag{4}$$

where D and n are material constants with D representing the limiting strain rate in shear and $J_2 = 1/2\ \underset{\sim}{S}\underset{\sim}{S}$.

A major difference between Eqs. (1) and (4) is that the back stress models assume the direction of the inelastic strain rate vector to be coincident with the direction of $(\underset{\sim}{S} - \underset{\sim}{\alpha})$ whereas the Bodner model assumes it to be coincident with direction of $\underset{\sim}{S}$.

Isotropic and directional hardening are distinguished by a partitioning of the internal variable Z into components Z_I and Z_D rather than by a back stress.

$$Z = Z_I + Z_D \tag{5}$$

The evolutionary equations for the internal variable are of the form

$$\dot{Z}_I = h_1(Z_1 - Z_I)\dot{W}_p - r_1 \tag{6}$$

$$\dot{Z}_D = h_2(Z_D)\dot{W}_p - d(Z_D)\dot{W}_p - r_2 \tag{7}$$

The constant Z_1 in Eq. (6) is the saturation value of Z_I. Cyclic hardening or softening is controlled by the Z_I component and depends on whether the initial value of Z_I is less than or greater than Z_1. The procedure for incorporating directional hardening in the theory was developed by Bodner during this program. Another difference between the evolutionary equations for the Bodner model and the back stress-drag stress type of model is that the former uses the plastic work rate, $\dot{W}_p$, as the measure of hardening rather than the inelastic strain rate. There are essentially nine material constants to be determined for the Bodner model, of which only three were found to be temperature-dependent.

Because of its unique form and its simplicity compared to the more common back stress models, the Bodner model was selected for more detailed study under both contractual efforts. Of the back stress-drag stress type of theory, both contractors selected the Walker model as a basis for further study. The reason for this selection was that the Walker model was further along in development for finite-element analysis than other comparable back stress-drag stress models. The major difficulty in applying the Walker model is to determine the 14 temperature-dependent material constants.

In the course of this study, Bodner and Walker (who were used as consultants in the SwRI/PWA program) incorporated additional terms in their models to account for nonproportional loading. As the measure of nonproportionality, Bodner used the angle between the stress and stress rate directions while Walker used the angle between the strain and

strain rate directions. Walker also revised his model to use an exponential law in place of the previous power law for the functional form of the kinetic term, $f(\dot{\varepsilon}_I)$, in Eq. (1).

A composite of the two models was developed in the G.E. program with the purpose of retaining the basic simplicity of the Bodner model and using the directional hardening form of the Walker model. This involved incorporating a back stress in the flow law of the Bodner model to give

$$\dot{\underline{\varepsilon}}_I = D \exp\left[-\frac{A}{2}\left(\frac{Z^2}{3K_2}\right)^n\right]\frac{\underline{S} - \underline{\alpha}}{\sqrt{K_2}} \qquad (8)$$

where $K_2 = 1/2(\underline{S} - \underline{\alpha})(\underline{S} - \underline{\alpha})$ and A is a constant related to the activation energy. The back stress growth law for the composite model, as shown below, is essentially Eq. (3) with an additional function, g, to improve the modeling of the cycle in the elastic range.

$$\dot{\underline{\alpha}}^* = h_2(\underline{\alpha})\dot{\underline{\varepsilon}}_I - d(\alpha)\left|\dot{\underline{\varepsilon}}_I\right| - r_2 \qquad (9)$$

$$\underline{\alpha} = \left[1 - g(\alpha)\underline{\alpha}^* + g(\alpha)\underline{\alpha}\right] \qquad (10)$$

The directional form of Z given by Eq. (7) was eliminated. Isotropic hardening is described by the isotropic form of the Z variable given by the evolutionary Eq. (6). There are six material constants to be experimentally determined for the composite model, neglecting thermal recovery terms.

Evaluation of Constitutive Models

Evaluation of the candidate unified theories was based on extensive uniaxial and multiaxial testing. The parameters varied in these tests were temperature, strain rate, strain range, mean strain, dwell time and, for the multiaxial tests, stress field. Details of the test specimens, conditions, and procedures are described in the first annual reports[5,6] of the contractors. One of the significant differences between the two contract efforts was in the cyclic behavior of the base materials that were selected. The G.E. alloy, René 80, exhibited some cyclic softening at elevated temperatures while the SwRI/P&W alloy, B1900+Hf, underwent cyclic hardening. The discussion below is directed mainly toward the Bodner model for the SwRI program and the composite model for the G.E. program. Difficulties were encountered in both programs in determining the Walker model constants.

Bodner Model

All of the constants for the B1900+Hf alloy were obtained from uniaxial, monotonic, tensile stress-strain tests. These tests were conducted over a range of temperatures from room temperature up to 1093 °C and over a range of strain rates from 0.0005 to 0.1 min^{-1}. A comparison of the calculated and experimental stress-strain curves is shown in Fig. 1 at temperatures of 538, 871, and 982 °C for a strain rate of 0.005 min^{-1}. To determine the constants associated with strain hardening, the tensile data were correlated in terms of the derivative of the stress with respect to the plastic work plotted against stress, as shown in Fig. 2. The curves for each strain rate are seen to be essentially parallel. Each of these curves was approximated by two linear segments. From the slopes and intercepts of the segments, the isotropic (Z_I) and directional (Z_D) variables could be readily determined. The slopes will change with temperature at the higher temperatures due to thermal recovery effects (Eqs. (6) and (7)). For a cyclic softening material, this correlation would result in entirely linear curves and some cyclic tests would be required to determine the directional component (Z_D).

Cyclic response was successfully predicted for the B1900+Hf alloy using the material constants obtained from the monotonic tensile stress-strain tests. As shown in Fig. 3, the cyclic predictions during initial cycling and at saturation show excellent qualitative agreement with the experimental cycles.

An essential requirement for a unified theory is the capacity to characterize material creep behavior. This is demonstrated for the Bodner model in Fig. 4 where predicted and experimental results are compared for uniaxial, constant-load creep tests of B1900+Hf at various temperatures. As with the cyclic predictions presented in Fig. 3, the material constants were derived from monotonic tensile stress-strain tests at different strain rates.

The ability of the Bodner model to account for cyclic hardening under nonproportional loading is shown in Fig. 5. Comparison of the experimental (Fig. 5(a)) with the predicted (Fig. 5(b)) cyclic response of Hastelloy X tension-torsion specimens subjected to 90° out-of-phase loading indicate good correlation. The Bodner model always assumes coincidence between the deviatoric stress and plastic strain rate directions as shown in Fig. 6 while the tension-torsion test cycles had phase angles from 7° to 45°. However, this discrepancy in phase angle between the model assumptions and multiaxial experiments did not appear to adversely affect the accuracy of the cyclic predictions.

Walker Model

The material constants of the Walker model were less deterministic and more sensitive to the strain rate than the constants for the Bodner model. The model could predict the cyclic response for René 80 adequately provided a different set of constants was determined for several strain rates. This limitation in representing a range of strain rates for René 80 cyclic behavior applied to similar back stress-drag stress models that were investigated, but not to the composite model.

Cyclic stress-strain predictions for Hastelloy X under 90° out-of-phase tension-torsion loading (Fig. 5(c)) show good agreement with the experimental results. Although the predicted phase angles in Fig. 6 are 5° to 15° smaller than the experimental observations, this is more realistic than the assumption of coaxiality between the deviatoric stress and plastic strain rate vectors for the Bodner model. However, the theoretical results shown in Fig. 5(c) and Fig. 6 were obtained by fitting the Walker model to the experimental response in Fig. 5(a), whereas the Bodner

model predictions were based only on uniaxial monotonic test data in determining the material constants.

Composite Model

To better represent the cyclic softening behavior of René 80, G.E. developed a composite model which retained the functional form of the Bodner model but incorporated a Walker-type back stress in the constitutive equations. The growth law for this back stress was based on the inelastic strain rate as in the Walker theory while retaining the Bodner isotropic hardening variable based on the work hardening rate. All the material constants, except one, were determined from monotonic tensile stress-strain tests. The constant controlling the cyclic softening behavior was determined from saturated cyclic hysteresis loops. Figure 7 compares the calculated and experimental René 80 stress-strain curves at 982 °C for strain rates of 0.002, 0.02, 0.06, and 0.2 min^{-1}. The agreement is seen to be very good, especially considering the data scatter indicated by the two sets of tests at a strain rate of 0.2 min^{-1}.

Composite theory predictions of the high-temperature cyclic behavior of René 80 are compared with experimental hysteresis loops in Fig. 8 for fully reversed cycles at 982 °C. The stress-strain loops in Fig. 8(b) are for a relatively slow strain rate of 0.002 min^{-1} and in Fig. 8(a) for a high strain rate of 0.2 min^{-1}. The model predictions were able to capture the cyclic response reasonably well for both strain rates.

The composite model was also evaluated with respect to its ability to predict the creep characteristics of the material. In Fig. 9 inelastic strain calculations are compared to test data for constant load creep tests at 982 °C. As can be seen, the steady-state creep rate was reasonably predicted, but the primary creep rate was too high. The creep analysis capability of the model was also assessed for a strain controlled cycle involving stress relaxation, as shown in Fig. 10. In this test case, a 120 sec hold time was applied at the minimum strain limit of the cycle. Comparison of the analytical and experimental hysteresis loops show that the calculated minimum stress part of the cycle was too low, and as a consequence the calculated stress relaxation was too rapid. However, since the analytical and experimental loops were in agreement at the end of the stress relaxation, it appears that the model worked reasonably well in predicting the stress relaxation.

The composite model has been used to predict the response of René 80 at 982 °C under proportional and nonproportional multiaxial loading conditions. Figure 11(a) shows the stress behavior under a 90 degree out-of-phase tension-torsion cycling. It is seen that the model has the ability to analyze complex cyclic hardening and softening behavior under nonproportional loading conditions. Figure 11(b) shows the predicted phase angle between the inelastic strain rate and the deviatoric stress vectors. Comparison of Figs. 6 and 11 indicates that the phase angles are similar although the tests were very different. However, the loading conditions in the two multiaxial tests were similar and it has been found that the phase angle is a strong function of the loading condition. Further refinement of the composite model is expected as more multiaxial test data become available.

Implementation of Models in Finite-Element Codes

Unified constitutive theories involve mathematically stiff differential equations where small changes in the independent variables can cause large changes in the dependent variables. Successful implementation of unified theories in finite-element codes requires the use of efficient methods for integrating the constitutive equations. The suitability of any integration method is dependent on the iteration and incrementation algorithms used in the computer code and on the nature of the problems to be analyzed. In both contractual efforts an initial strain technique was employed for iterating the equilibrium equations. Since the constitutive flow law and the evolutionary equations are uncoupled, a further iteration is required within the overall equilibrium iteration to solve for the inelastic strain rate and internal variables. The iteration process causes the solution to tend to drift from the equilibrium state. To correct for this drift, residual load corrections are applied to the incremental loads by computing the difference between the external and internal forces summed over all the elements at the end of the previous increment. Automatic time incrementation has also been incorporated in the incrementation procedures to allow for time step control under large cyclic stress and inelastic strain excursions. The control is achieved by limiting the maximum stress and inelastic strain change permitted for any time increment.

General Electric developed both two- and three-dimensional nonlinear finite-element codes. These codes are modular and incorporated different inelastic constitutive models. A dynamic time incrementation procedure is used to minimize cost. The constitutive equations are integrated using a second order Adams-Moulton predictor-corrector technique. The number of iterations required has been reduced by improving the stability of the initial strain procedure. Figure 12 shows the analysis of an Inconel 718 benchmark notch specimen[7] using the Bodner model with the two-dimensional code. It can be seen that the code not only performed well, but provided excellent agreement with the measured notch root strains.

In the SwRI/P&W program, the constitutive equations for both the Bodner and revised Walker models, as well as the computational algorithms, were incorporated in the MARC user subroutine, Hypela. With some modifications this subroutine can become a stand-alone module for use with other general purpose nonlinear codes. A number of methods for integrating the Bodner and Walker constitutive equations are still being studied. An explicit Euler technique with a self-adaptive solution method has been found to be suitable for both models.

Concluding Remarks

The continuing development and revisions of unified constitutive material theories, as well as differences in the cyclic behavior of the materials studied makes difficult any definitive judgement at this point in the program as to which

constitutes the best approach. However, the results up to the present time give encouragement that this program will meet its objective to significantly advance the structural analysis capabilities for engine hot section components. These improvements in the structural analysis tools should provide better life prediction capability and greater hot section durability for the next generation of gas turbine engines.

References

1. McKnight, R.L., Laflen J.H., and Spamer, G.T., "Turbine Blade Tip Durability Analysis," General Electric Co., Cincinnati, OH, R81AEG372, Feb. 1981. (NASA CR-165268).

2. Moreno, V., "Combustor Liner Durability Analysis," Pratt and Whitney Aircraft Group, East Hartford, CT, PWA-5684-19, Feb. 1981. (NASA CR-165250).

3. Bodner, S.R., and Partom, Y., "Constitutive Equations for Elastic-Viscoplastic Strain-Hardening Materials," Journal of Applied Mechanics, Vol. 42, June 1975, pp. 385-389.

4. Walker, K.P., "Research and Development Program for Non-Linear Structural Modeling with Advanced Time-Temperature Dependent Constitutive Relationships," United Technologies Research Center, East Hartford, CT, PWA-5700-50, Nov. 1981. (NASA CR-165533).

5. Lindholm, U.S., Chan, K.S., Bodner, S.R., Weber, R.M., Walker, K.P., and Cassenti, B.N., "Constitutive Modeling for Isotropic Materials (HOST)," Southwest Research Institute, San Antonio, TX, SwRI 06-7576/13, May 1984. (NASA CR-174718).

6. Ramaswamy, V.G., Van Stone, R.H., Dame, L.T., and Laflen, J.H., "Constitutive Modeling for Isotropic Materials," NASA CR-17485, 1984.

7. Domas, P.A., Sharpe, W.N., Ward, M., and Yau, J., "Benchmark Notch Test Life Prediction," General Electric Co., Cincinnati, OH, R82AEB358, Oct. 1982. (NASA CR-165571).

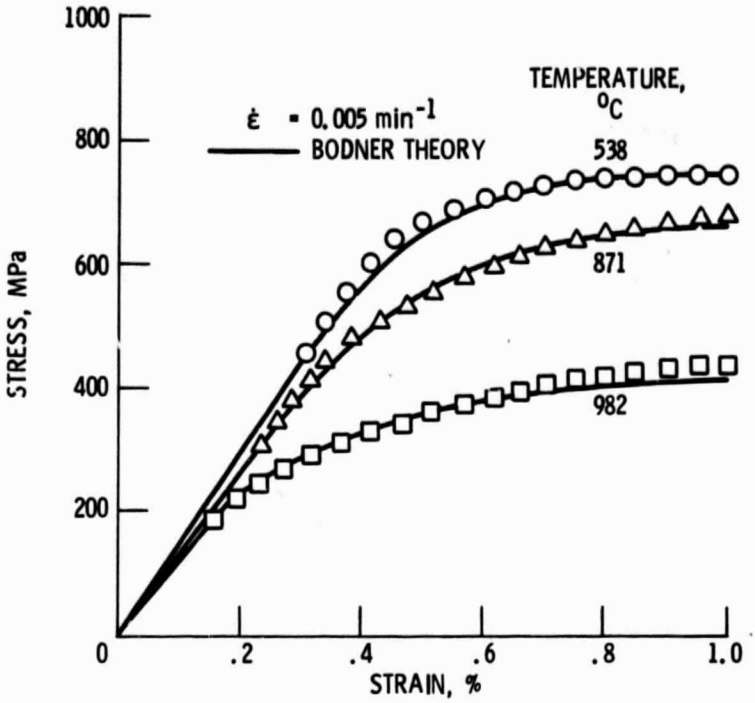

Figure 1. - A comparison of the calculated (Bodner theory) and the experimental stress-strain curves of B1900+Hf at 538, 871 and 982 °C.

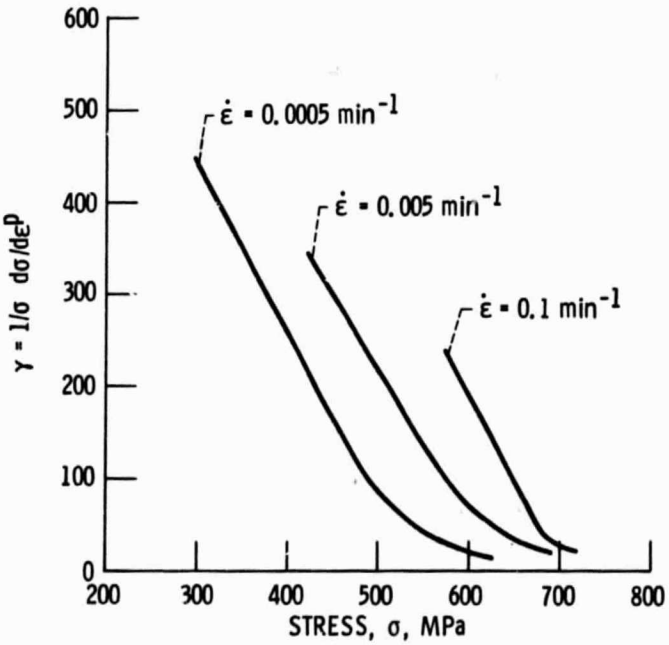

Figure 2. - Work hardening behavior of B1900+Hf at 871 °C.

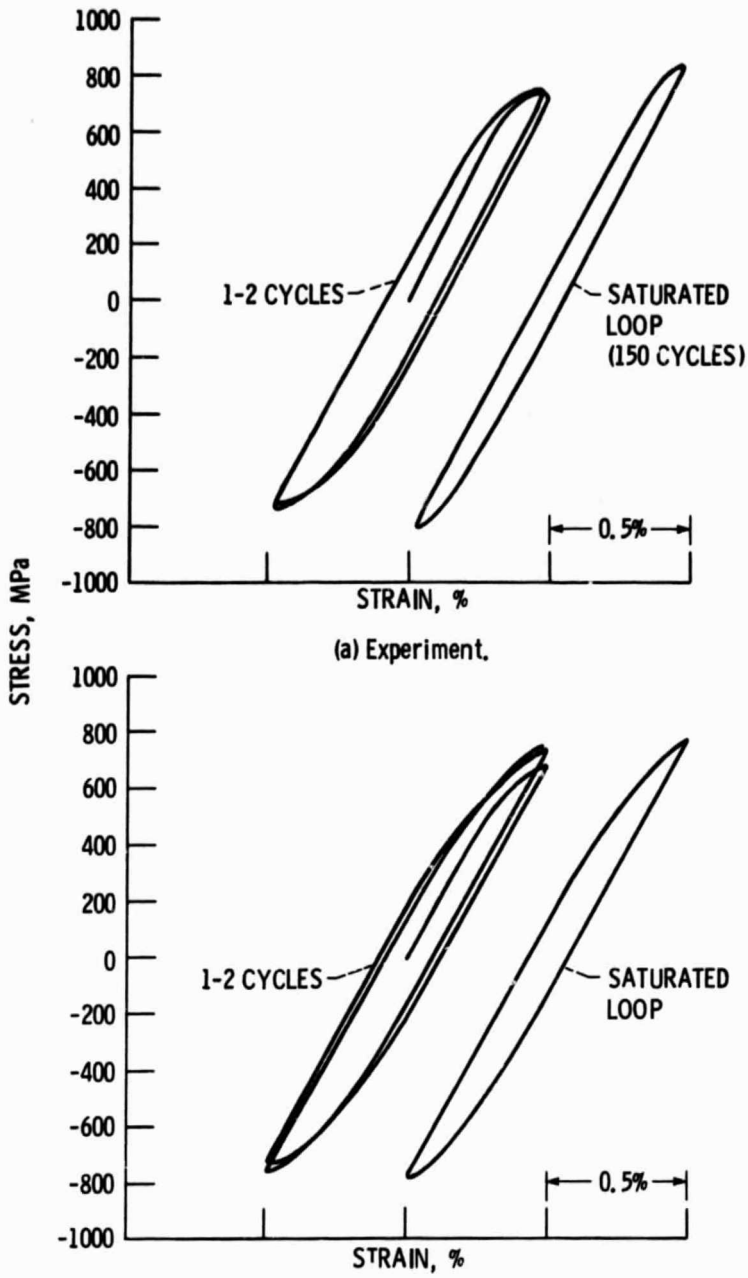

Figure 3. - A comparison of the calculated (Bodner theory) and the experimental hysteresis loops after 1-2 cycles and at cyclic saturation for B1900 + Hf at 538 ^{0}C and a strain rate of 0.05 min^{-1}.

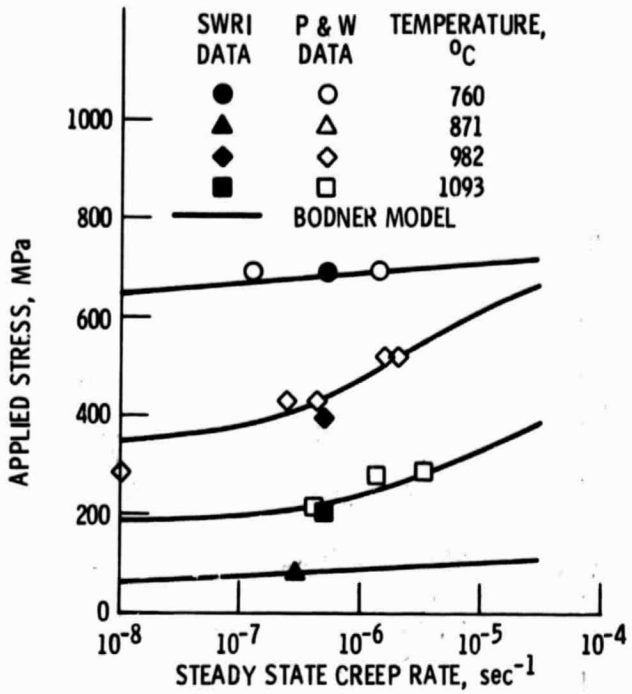

Figure 4. - Results from constant load creep tests for B1900 + Hf.

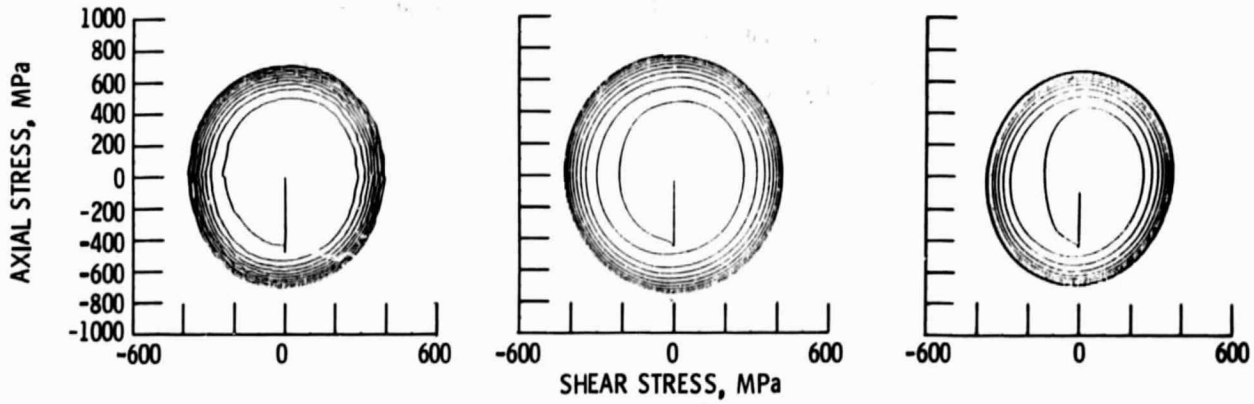

(a) Experimental data. (b) Bodner theory. (c) Walker theory.

Figure 5. - A comparison of Bodner and Walker theories with experimental results on the stress-strain response of Hastelloy-X tested under 90^0 out-of-phase tension/torsion loading at room temperature.

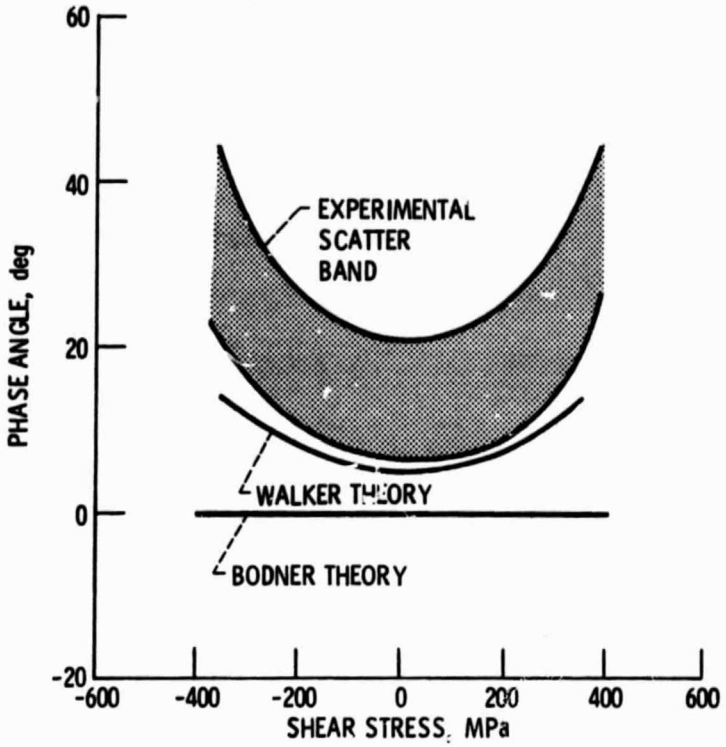

Figure 6. - A comparison of Bodner and Walker theories with experimental results on the phase angle between the deviatoric stress and the plastic strain rate vectors observed in Hastelloy-X tested under 90^{o} cut-of-phase tension/torsion loading at room temperature.

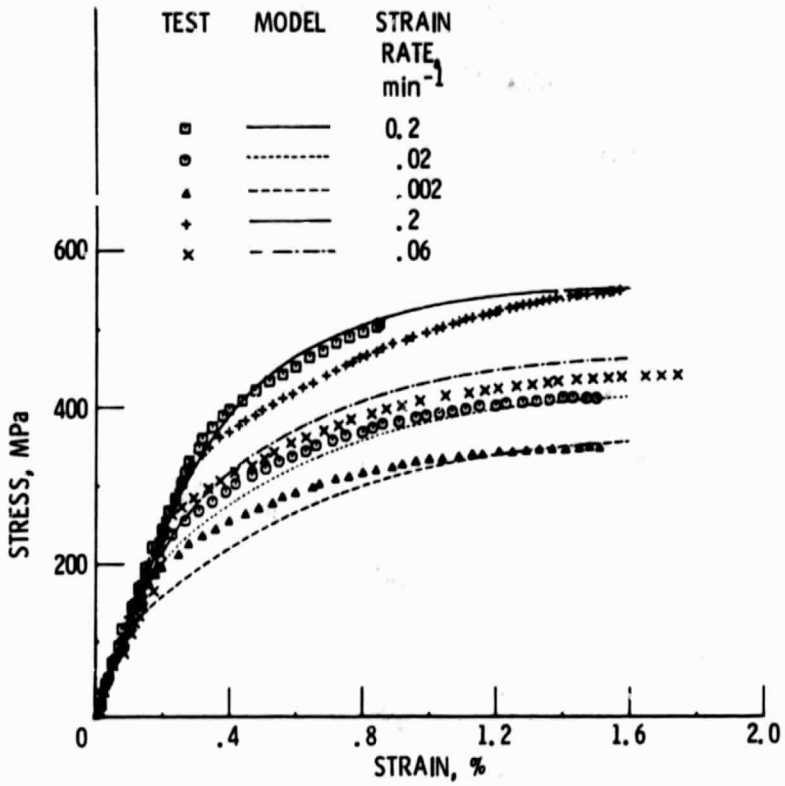

Figure 7. - A comparison of the calculated (composite theory) and the experimental stress-strain curves of Rene 80 at 982 ^{o}C.

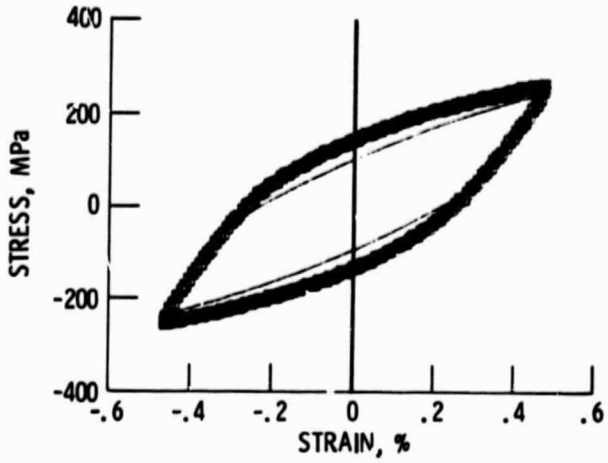

(a) Strain rate = 0.002 min^{-1}.

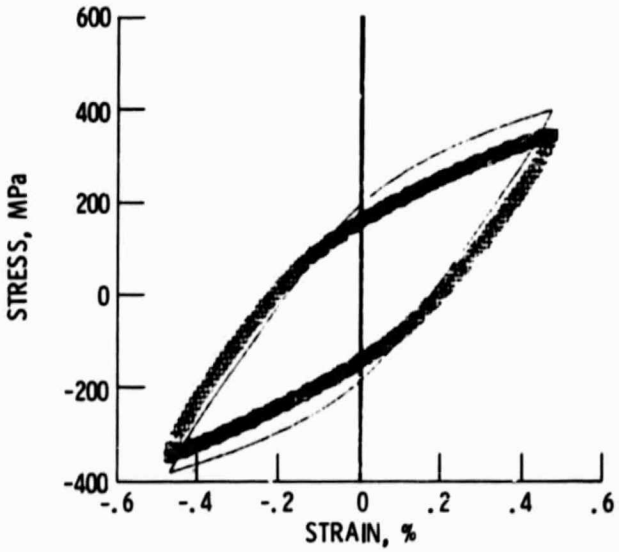

(b) Strain rate = 0.2 min^{-1}.

Figure 8. - A comparison of the calculated (composite theory) and the experimental hysteresis loops for Rene 80 at 982 ^{o}C.

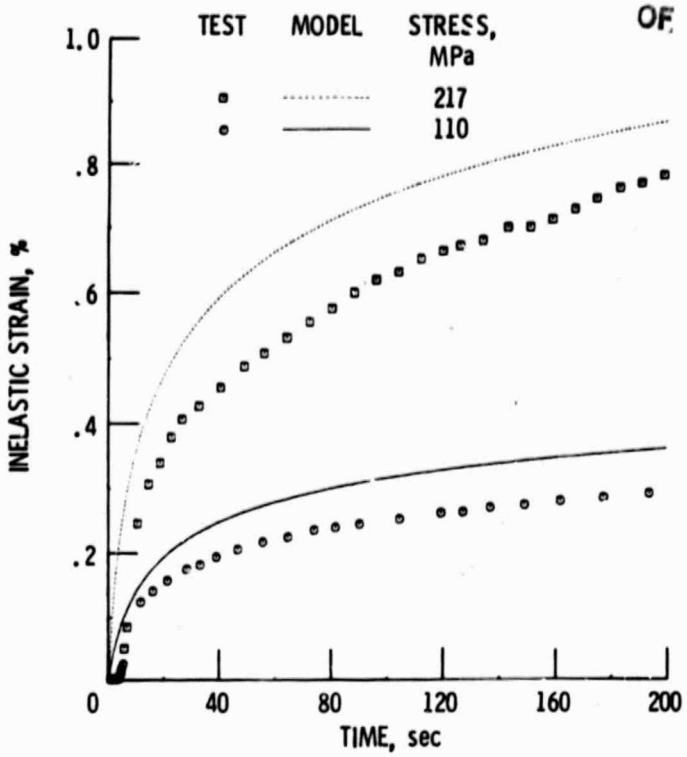

Figure 9. - Results from constant load creep tests of Rene 80 at 982 ^{0}C.

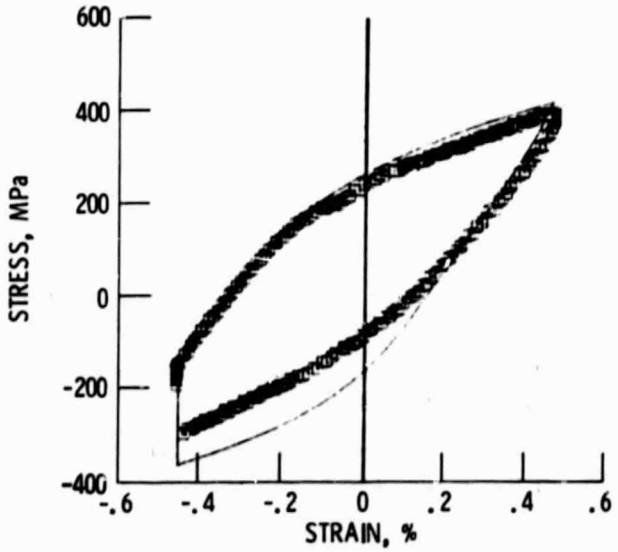

Figure 10. - A comparison of the calculated (composite theory) and the experimental hysteresis loops with 120 sec. hold time at minimum strain for Rene 80 at 982 ^{0}C.

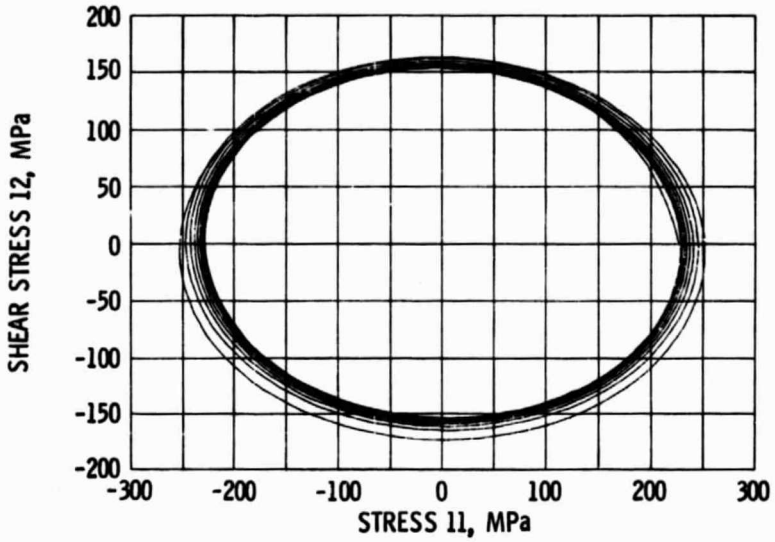

(a) Cyclic softening behavior.

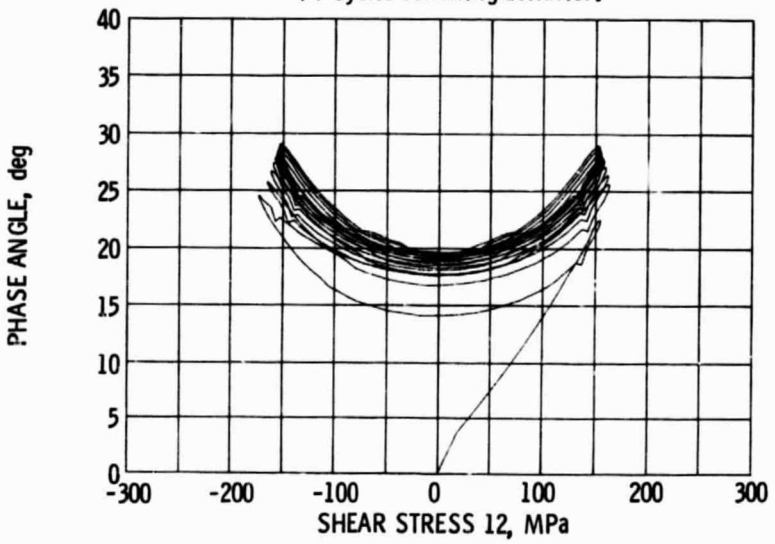

(b) Phase angle between the deviatonic stress and inelastic strain rate vectors.

Figure 11. - Composite model predictions of Rene 80 at 982 ^{0}C under 90^{0} out-of-phase tension/torsion loading.

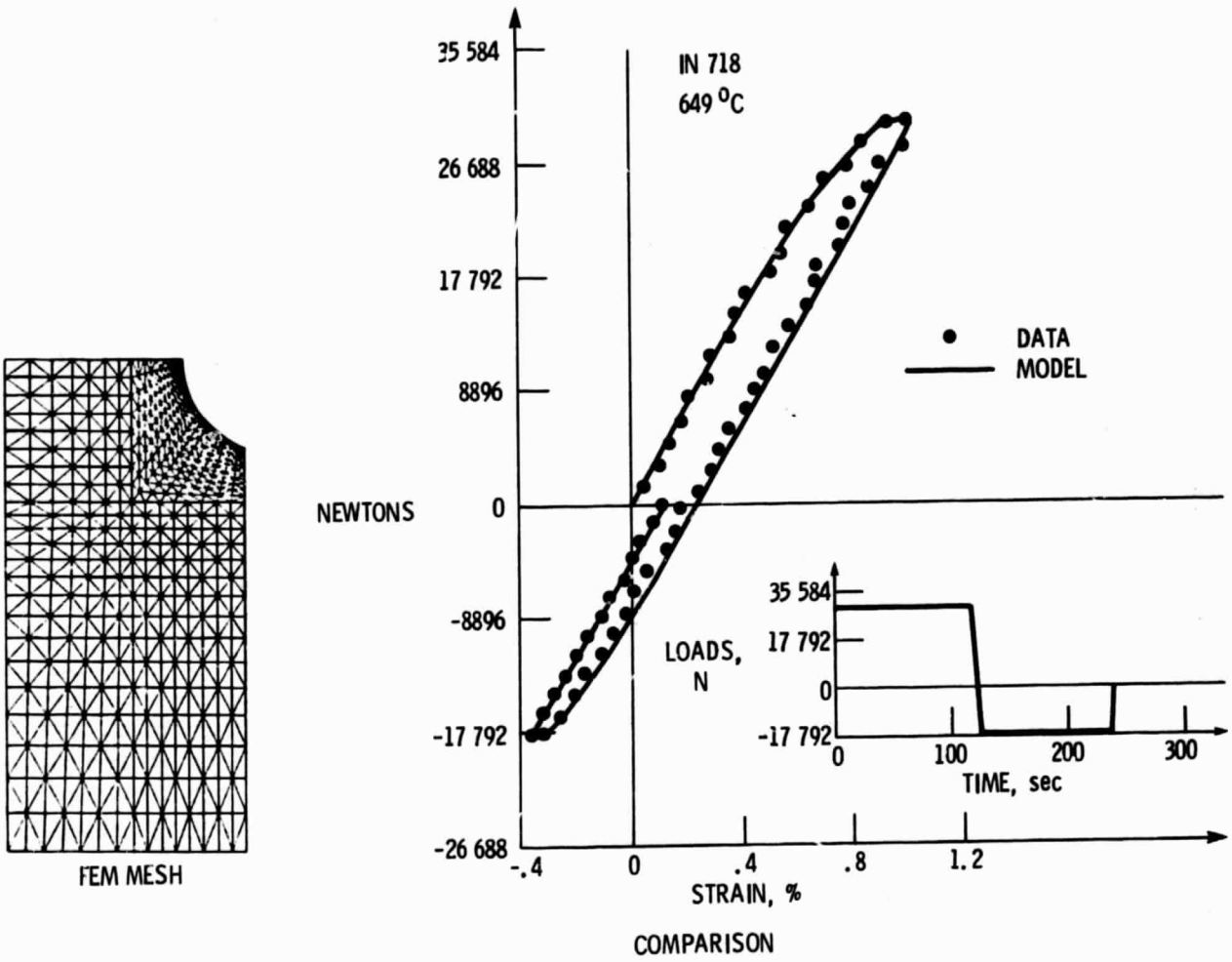

Figure 12. - Comparison of predicted and measured notch root strains using the Bodner model with 2 D computer code developed at General Electric.